

Investigation of the ideal composition of metal hexacyanocobaltates with high water oxidation catalytic activity

Ferdî KARADAŞ^{1,2,*} ¹Department of Chemistry, Bilkent University, Ankara, Turkey²UNAM-Institute of Materials Science and Nanotechnology, Bilkent University, Ankara, Turkey

Received: 18.04.2018

Accepted/Published Online: 24.12.2018

Final Version: 03.04.2019

Abstract: The electrocatalytic activities of Prussian blue analogues (PBAs) have recently received much attention due to their robustness and efficiency. Considering that PBAs with hexacyanocobaltate building block stand forward among other PBAs, a systematic study on a family of metal hexacyanocobaltates is presented in this study. Metal hexacyanocobaltates (M = Co, Mn, Ni, and Fe) were prepared, characterized, and electrochemical studies were performed. A series of mixed-metal cobalt-iron hexacyanocobaltates has also been studied to determine the ideal composition of a metal hexacyanocobaltate for electrocatalytic water oxidation process. The overall study clearly indicates that cobalt hexacyanocobaltate exhibits the highest electrocatalytic activity among all.

Key words: Prussian blue, cyanide, water oxidation, electrocatalysis

1. Introduction

The concept of hydrogen economy, which mainly involves the splitting of water using solar energy, has received intense interest in the last two decades since it is a clean and renewable source of energy.^{1–4} Water oxidation, the half reaction of water splitting, is considered to be one of the main challenges in this cycle. Much effort has been devoted to the development of efficient and robust water-oxidation catalysts (WOCs) that are composed of earth-abundant elements.^{5–7} Given the recent advances in CoPi catalysts, cobalt oxide-based catalysts have been studied extensively.⁸ Even though cobalt oxide catalysts could oxidize water at relatively lower overpotentials, their instabilities in acidic media stimulates research on nonoxide cobalt based heterogeneous catalysts for water oxidation. Berlinguette et al. have recently reported a molecular water-oxidation catalyst with a single cobalt site coordinated to a pentadentate N-donor ligand and a water molecule.⁹ This study has shown that not only a single metal site could oxidize water with a remarkably high catalytic efficiency than conventional amorphous cobalt oxides, but also cobalt sites surrounded with nitrogen atoms have superior stabilities even in acidic media. Cobalt corrole hangman complexes, reported the same year by Nocera et al., also exhibit higher turnover frequencies compared to cobalt oxides-based systems.¹⁰ Furthermore, cobalt-nitrogen matrices incorporated into coordination networks have recently been observed to have promising potential as water oxidation and reduction catalysts.^{11,12} For example, a current density of 1 mA cm⁻² could be obtained with cobalt cyanamides at an overpotential of 490 mV and they maintain a stable current density over an electrolysis of 20 h.¹³ The stability of nonoxide cobalt-based systems over long durations of electrolysis has also been observed with cobalt hexacyanoferrate (CoHCF).^{14–18} CoHCF is a member of one of the well-known family of compounds, Prussian

*Correspondence: karadas@fen.bilkent.edu.tr

Blue analogues (PBAs), which adopt a cubic structure wherein metal sites are connected to each other with cyanide bridging groups.¹⁹ PBAs have unique features, which make them ideal candidates as water-oxidation catalysts: i) they are made of earth-abundant elements, ii) their compositions could easily be tuned due to their well-established easy preparation, iii) they retain their network structures in neutral and basic media in addition to acidic medium, and iv) they have comparable turnover frequencies to those of cobalt oxides. Moreover, the versatility of PBAs can be used for the fundamental understanding of water oxidation. For example, our group has recently studied a series of cobalt hexacyanometalates ($\text{Co}_x[\text{M}(\text{CN})_6]$ $\text{M} = \text{Fe}^{2+/3+}, \text{Co}^{3+}, \text{Cr}^{3+}$) to investigate the effect of $[\text{M}(\text{CN})_6]$ group on the catalytic activity of cobalt sites.²⁰ It has been shown that the type of $[\text{M}(\text{CN})_6]$ fragment can significantly change the electron density and thus the electrocatalytic activity of cobalt sites. The highest catalytic activity was obtained with $\text{Co}_3[\text{Co}(\text{CN})_6]_2$. Given the aforementioned result, this study aims to perform a systematic study on a series of metal hexacyanocobaltates, $\text{M}_x[\text{Co}(\text{CN})_6]$ ($\text{M} = \text{Co}, \text{Mn}, \text{Fe}, \text{and Ni}$), to investigate the effect of metal site on this series. Since cobalt and iron derivatives exhibit the highest electrocatalytic activities among all, the effect of the addition of iron impurities on cobalt hexacyanocobaltates has been investigated by preparing a series of mixed-metal hexacyanocobaltates. Cyclic voltammetric and chronoamperometric studies have been performed to investigate and compare their electrocatalytic activities.

2. Results and discussion

2.1. Synthesis and characterization

Four metal hexacyanoferrate compounds, $\text{M}[\text{Co}(\text{CN})_6]_{0.67}$ (abbreviated as $[\text{Mn-Co}]$, $[\text{Fe-Co}]$, $[\text{Co-Co}]$, $[\text{Ni-Co}]$ throughout the manuscript), were synthesized via a straightforward precipitation method.²⁰ Furthermore, two mixed metal hexacyanometalates, $\text{Co}_{0.9}\text{Fe}_{0.1}[\text{Co}(\text{CN})_6]_{0.67}$ (abbreviated as $[\text{Co}_{0.9}\text{Fe}_{0.1}\text{-Co}]$) and $\text{Co}_{0.5}\text{Fe}_{0.5}[\text{Co}(\text{CN})_6]_{0.67}$ (abbreviated as $[\text{Co}_{0.5}\text{Fe}_{0.5}\text{-Co}]$), were prepared using a similar procedure.

Powder XRD studies were performed on powder samples of derivatives to investigate their crystalline nature. XRD patterns displayed in Figure 1 clearly indicate that all samples adopt identical Prussian blue crystal structure. All samples exhibit a sharp diffraction peak at around 17° (2θ) indicating formation of a cubic $\text{Fm}\bar{3}\text{m}$ unit cell with a lattice parameter of around 10.1 \AA .

Infrared spectroscopy is one of the reliable techniques for the characterization of PBAs since cyanide

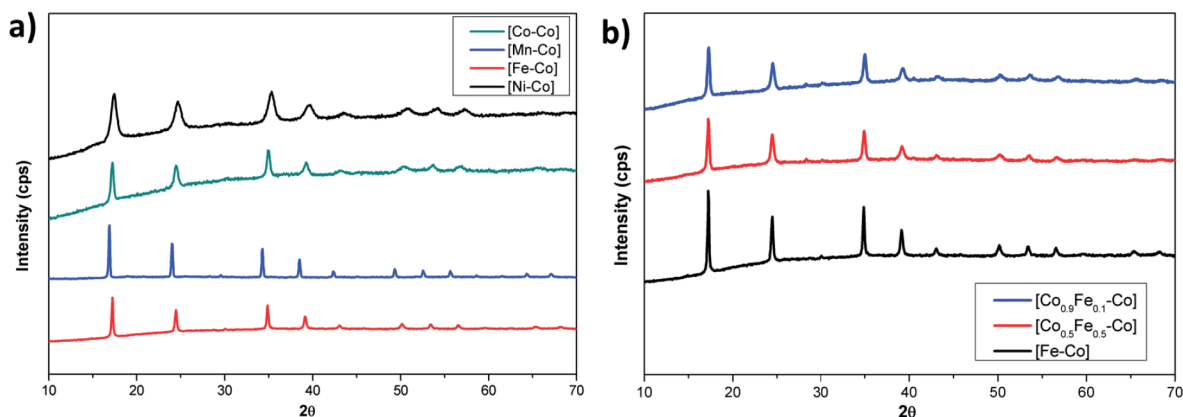


Figure 1. XRD patterns for a) metal hexacyanocobaltates and b) mixed-metal hexacyanometalates.

stretch is highly dependent on the coordination mode and the oxidation states of the metal ions coordinated. Cyanide acts as a σ -donor (by donating electrons to the metal) as well as a π -acceptor (accepting electrons from a metal). The σ donation ability of the cyanide, however, is dominating its π -acceptor character because of the negative charge. A blue shift is observed in ν CN stretch with the removal of electrons from the weakly antibonding σ -molecular orbital (increased σ -donation) while conversely it tends to show red shift with the addition of electrons into the π -bonding orbital (decreased π -acceptance properties).^{19,21} FTIR spectra (Figure 2) of each compound exhibit sharp peaks in the 2150–2180 cm^{-1} range. The CN^- stretching frequency shifts to higher frequencies (compared to $[\text{Co}(\text{CN})_6]^{3-}$ complex) due to coordination of Co^{2+} ions to the nitrogen atoms of cyanide ligands (Figure 2),²² which can be attributed to the M-NC-Co^{III} coordination mode. A peak is obtained at 439, 450, 451, and 490 cm^{-1} , respectively, for [Mn-Co], [Fe-Co], [Ni-Co], and [Co-Co], which is attributed to M-C bond stretch. It is also evident from the infrared spectra that each compound has interstitial water molecules since all spectra exhibit a sharp stretch at around 1608 cm^{-1} and a broad one at 3400 cm^{-1} , which correspond to H-OH bending and O-H stretch, respectively.

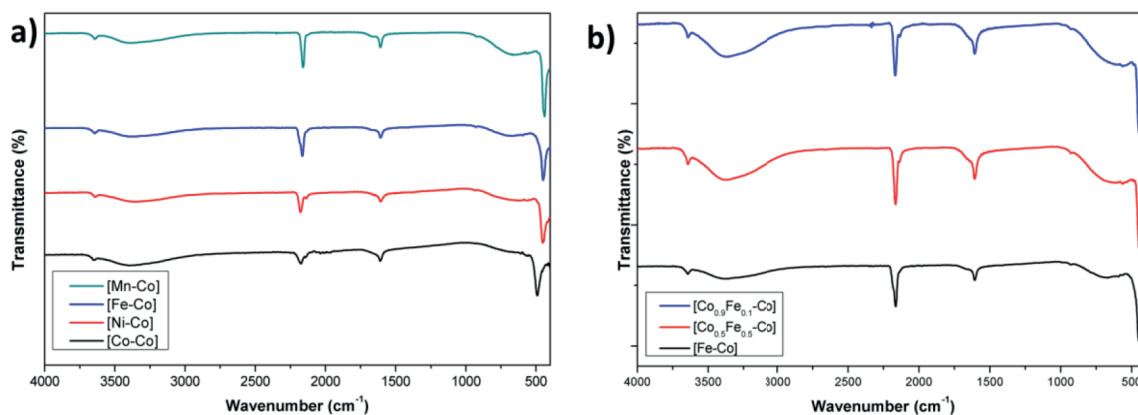


Figure 2. Infrared spectra for a) metal hexacyanocobaltates and b) mixed-metal hexacyanocobaltates.

2.2. Water oxidation studies

Cyclic voltammograms (CV) of PBA-coated fluorine doped tin oxide (FTO) electrodes were performed in phosphate buffer (KPi) solution (pH 7) using 1M KNO_3 as an electrolyte in the range of 0–1.5 V vs. Ag/AgCl reference electrode and at a scan rate of 50 mV s^{-1} (Figure 3). All compounds exhibit irreversible peaks at high anodic potentials, which correspond to the catalytic water oxidation process. The comparison of CV profiles indicates that [Co-Co] exhibits the lowest overpotential and thus the highest catalytic activity, among all. [Fe-Co] and [Co-Co] exhibit similar performances at high anodic potentials. [Mn-Co] and [Ni-Co], however, exhibit much higher overpotentials for catalytic water processes. The comparison clearly shows that the catalytic activity trend in metal hexacyanocobaltates is: $\text{Co} > \text{Fe} > \text{Mn} \sim \text{Ni}$.

Our further electrochemical experiments were focused on [Fe-Co], [Co-Co], and their mixed metal hexacyanocobaltate derivatives since cobalt and iron sites exhibit promising electrocatalytic activities. The CVs of PBAs are displayed in Figure 4. Interestingly, $[\text{Co}_{0.9}\text{Fe}_{0.1}\text{-Co}]$ exhibits a lower overpotential than [Co-Co], which implies that the substitution of cobalt impurities with iron impurities could lead to an increase in the electrocatalytic activity.

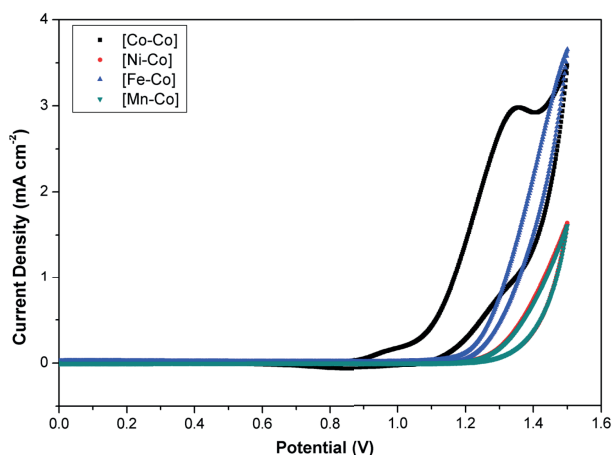


Figure 3. CV of PBA modified FTO electrodes recorded in a phosphate buffer solution with 1 M KNO_3 as electrolyte at $\text{pH} = 7.0$ with a 50 mV/s sweep rate.

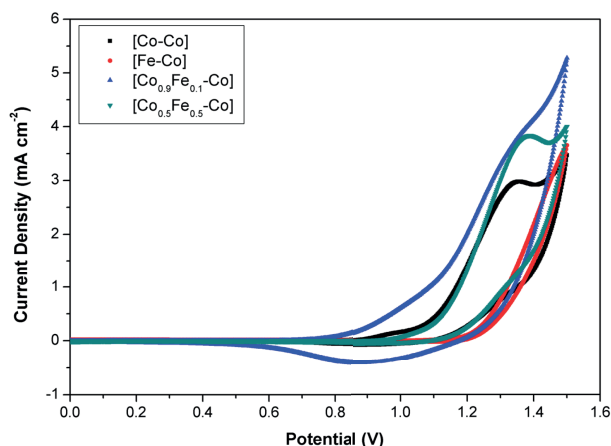


Figure 4. CV of PBA modified FTO electrodes recorded in a phosphate buffer solution with 1 M KNO_3 as electrolyte at $\text{pH} = 7.0$ with a 50 mV/s sweep rate.

It is also apparent from CVs that cobalt-based PBAs exhibit quasireversible peaks at around ~ 0.9 V (vs Ag/AgCl), which is attributed to $\text{Co}^{2+}/^{3+}$ redox process. CVs with different scan rates were recorded in the region of $\text{Co}^{2+}/^{3+}$ redox couple to determine the coverage of redox-active Co centers on the electrode, i.e. surface concentration (Figure 5). The surface concentrations (Γ) of $[\text{Co}_{0.9}\text{Fe}_{0.1}\text{-Co}]$ and $[\text{Co}_{0.5}\text{Fe}_{0.5}\text{-Co}]$ were extracted from the slope of current density (j) vs. scan rate plots, which are 2.21 and 1.90 nmol cm^{-2} , respectively. The surface concentration of $[\text{Co-Co}]$ was found to be equal to 2.40 nmol cm^{-2} in our previous study.²⁰ The trend clearly shows that surface concentration decreases gradually as the amount of cobalt in PBA derivatives decreases.

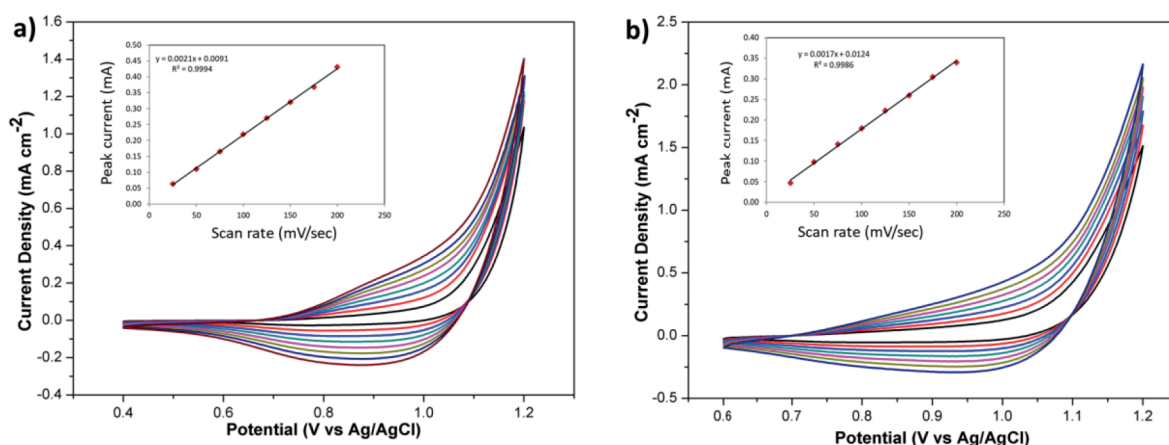


Figure 5. CV of a) $[\text{Co}_{0.9}\text{Fe}_{0.1}\text{-Co}]$ and b) $[\text{Co}_{0.5}\text{Fe}_{0.5}\text{-Co}]$ modified FTO electrodes recorded at different scan rates (25–200 mV/s with 25 mV/s increments). The insets show the linear trend between peak current and scan rate. Experiments were performed in a phosphate buffer solution with 1 M KNO_3 as electrolyte at $\text{pH} = 7.0$.

Chronoamperometry measurements were performed to investigate the catalytic activity of mixed-metal PBAs to obtain their Tafel slopes. The experiments were held in 50 mM KPi buffer solution with 1 M KNO_3 as electrolyte, at $\text{pH} 7$, and the potential was increased with 0.02 V increments to obtain a Tafel slope for each

derivative (Figure 5). A linear trend was obtained in the 300–450 mV region. The deviation from linearity is attributed to the absence of a catalytic process while the one at higher overpotentials is due to formation of O₂ bubbles on the electrode surface. Tafel slopes (Figure 6) of [Co-Co]-, [Co_{0.9}Fe_{0.1}-Co]-, [Co_{0.5}Fe_{0.5}-Co]-, and [Fe-Co]-coated FTO electrodes were found to be 99, 104, 104, and 112 mV/decade, respectively. The slopes are comparatively higher than the previously reported CoPi catalyst film²³ and cobalt-sulfide catalyst,²⁴ while it is similar to those obtained for Co/Fe Prussian blue catalysts,²⁵ in situ-generated copper oxide film from [Cu(triethanol-amine)(H₂O)₂][SO₄] complex,²⁶ and cobalt carbodiimide (CoNCN).²⁷ The similarity in Tafel slopes indicates that all PBAs oxidize water via a similar catalytic mechanism. Catalytic current densities of 55 μA cm⁻² (η_{onset}) and 1 mA cm⁻² (η_{1mA}) were also extracted from Tafel slopes. These overpotentials increase as the amount of cobalt decreases. The catalytic onset overpotentials of cobalt-based PBAs are within the range reported for Co/Pi ($\eta = 280$ mV), CoNCN ($\eta = 320$ mV), and Co(PO₃)₂ ($\eta = 310$ mV).^{23,27,28} Overpotentials for 1 mA cm⁻² are much lower than the ones reported for Co/Fe Prussian blue catalysts ($\eta > 600$ mV).²⁵ and MnOx catalysts.²⁸ Table summarizes the catalytic performances of mixed-metal hexacyanocobaltates. Overall, the measurements indicate that [Co-Co] exhibits the highest catalytic activity. log TOF vs. η plots for [Co_{0.9}Fe_{0.1}-Co] and [Co_{0.5}Fe_{0.5}-Co] were extracted by converting Tafel plots using surface concentration data (Figure 7). A turnover frequency (TOF) of 2.6×10^{-3} s⁻¹ could be achieved at an overpotential of 262 mV while it is 295 and 312 mVs for [Co_{0.9}Fe_{0.1}-Co] and [Co_{0.5}Fe_{0.5}-Co], respectively. A trend similar to surface concentration was obtained as expected.

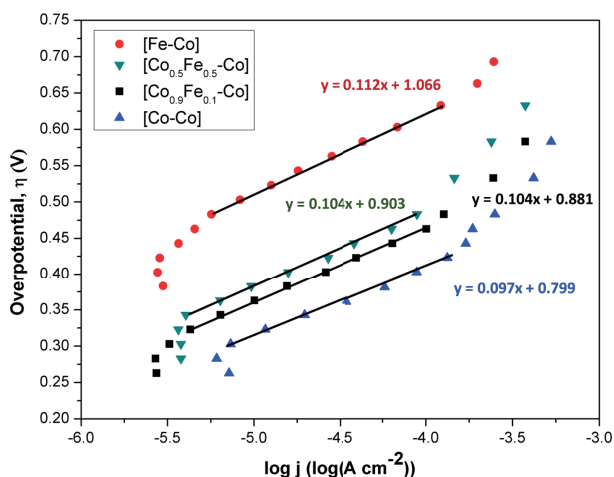


Figure 6. Tafel slopes for [Co-Co], [Co_{0.9}Fe_{0.1}-Co], [Co_{0.5}Fe_{0.5}-Co], and [Fe-Co] obtained in 50 mM KPi buffer solution with 1 M KNO₃ as electrolyte at pH 7.

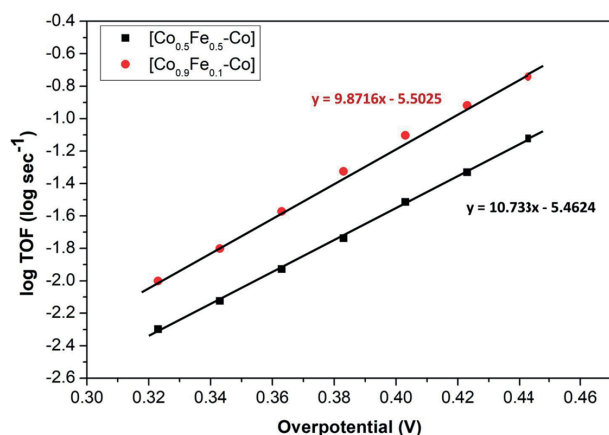


Figure 7. log TOF vs. η plots for [Co_{0.9}Fe_{0.1}-Co] and [Co_{0.5}Fe_{0.5}-Co] extracted from Tafel plots at pH 7.

Long-term chronoamperometry studies at pH = 7 was performed for [Co_{0.9}Fe_{0.1}-Co], [Co_{0.5}Fe_{0.5}-Co], and [Fe-Co] to assess their stabilities throughout a 30 h electrocatalytic process (Figure 8). Similar to [Co-Co] reported previously, the current decreases gradually with time. Once the electrolyte is refreshed and the experiment is restarted, a similar profile is obtained, which indicates that the catalyst is stable and retains its structural integrity during the catalytic process. The similarity in the cyclic voltammetric profiles obtained before and after chronoamperometry experiment also supports this thesis. Furthermore, XPS studies were performed to confirm the stability of the catalyst (Figure 9). A possible product is considered to be a metal

Table. Comparison of structural parameters and electrocatalytic performances of mixed-metal hexacyanocobaltates.

Sample	Surface concentration (nmol cm ⁻²)	CN stretch (cm ⁻¹)	Lattice parameter (Å)	η_{onset} (V)	Tafel slope (mV dec ⁻¹)	η_{1mA} (V)
[Co-Co]	2.4	2176	10.11	283	99	531
[Co _{0.9} Fe _{0.1} -Co]	2.21	2168	10.09	303	104	569
[Co _{0.5} Fe _{0.5} -Co]	1.90	2165	10.16	323	104	591
[Fe-Co]	none	2164	10.16	475	112	730

oxide species when PBAs decompose under applied bias. The absence of an additional peak at higher binding energies in the O1s region rules out the possibility of decomposition. The similarity of the O1s region for the pristine and postcatalytic electrodes also confirm the stability of the catalyst.

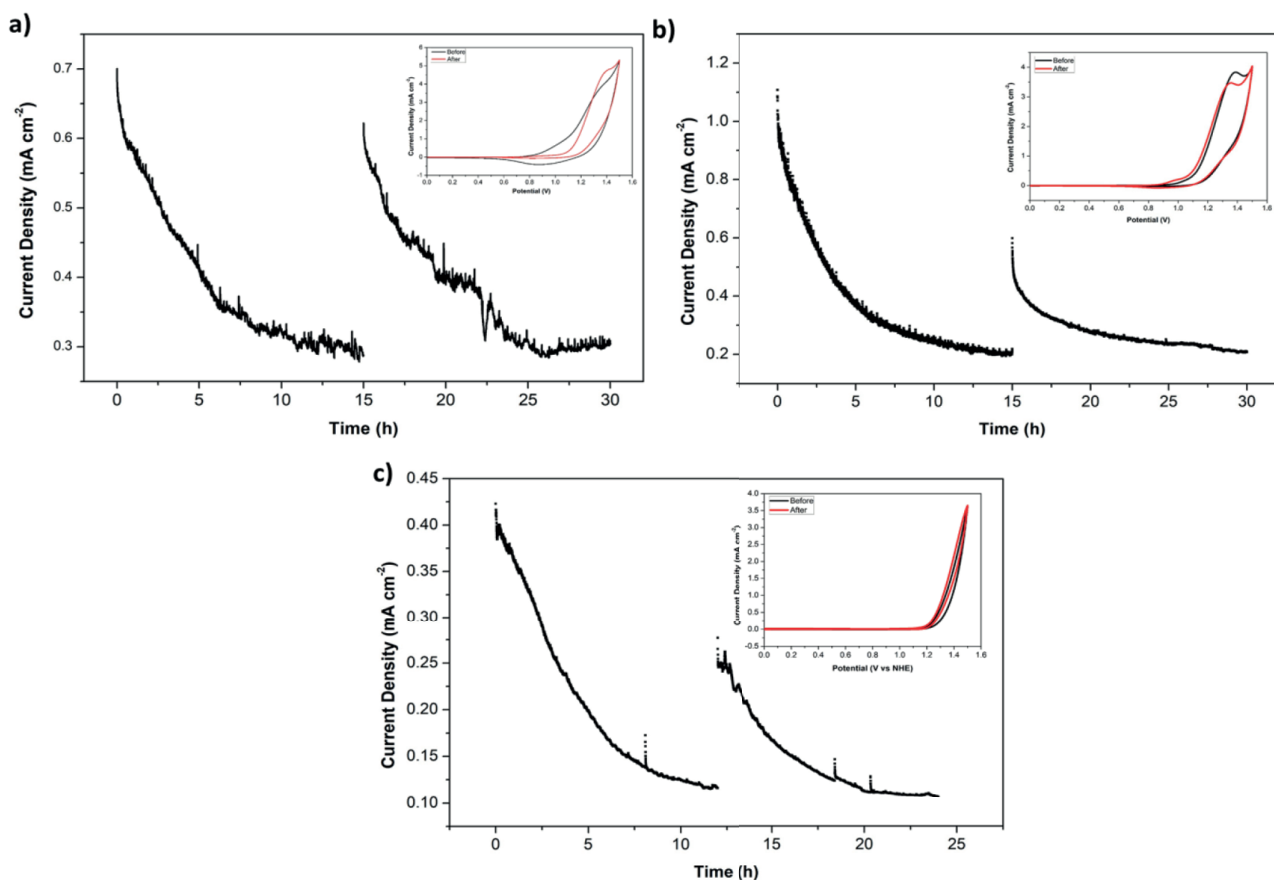


Figure 8. Long term electrolysis studies for [Co-Co], [Co_{0.9}Fe_{0.1}-Co], [Co_{0.5}Fe_{0.5}-Co], and [Fe-Co] performed at 1.2 V (vs. Ag/AgCl electrode) recorded in 50 mM KPi electrolyte at pH = 7.0. The insets display the cyclic voltammetric profiles before and after electrolysis.

2.3. Conclusions

A systematic study on a series of metal hexacyanocobaltates has been performed for the first time. All PBAs are isostructural, which make them ideal to study the effect of metal on the electrocatalytic activity.

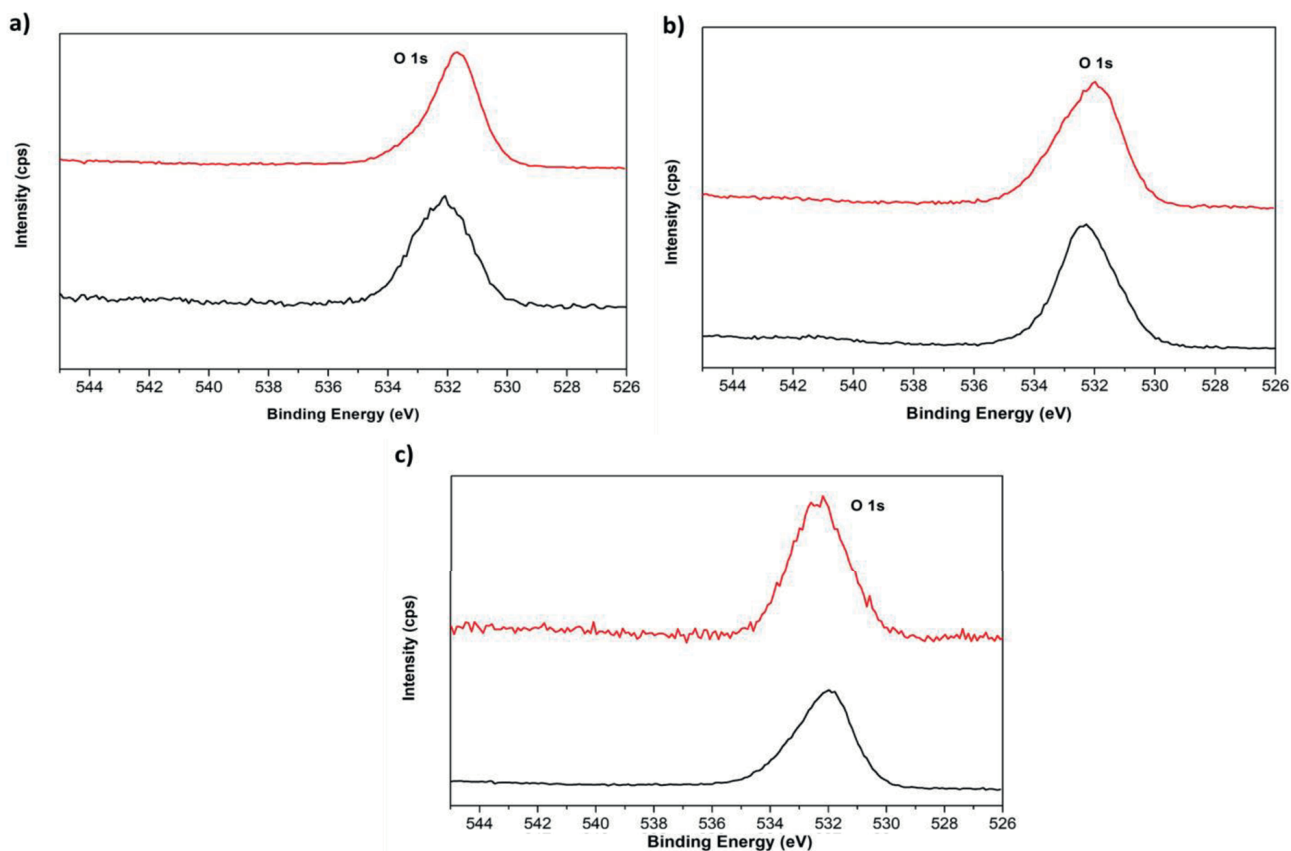


Figure 9. O1s region for pristine (black) and postcatalytic (red) electrodes for a) $[\text{Co}_{0.9}\text{Fe}_{0.1}\text{-Co}]$, b) $[\text{Co}_{0.5}\text{Fe}_{0.5}\text{-Co}]$, and c) $[\text{Fe-Co}]$ obtained by XPS studies.

Since $[\text{Co-Co}]$ and $[\text{Fe-Co}]$ exhibit relatively higher catalytic activities, a further study on mixed cobalt-iron hexacyanocobaltates has been designed by preparing PBAs with 10% ($[\text{Co}_{0.9}\text{Fe}_{0.1}\text{-Co}]$) and 50% ($[\text{Co}_{0.5}\text{Fe}_{0.5}\text{-Co}]$) iron impurities. This approach, which has been used previously by us with metal dicyanamides, indicates that both surface concentration and electrocatalytic activity decrease gradually as the amount of cobalt in PBAs decreases. The trend clearly shows that cobalt sites in Prussian blue networks are the most active catalytic sites for water oxidation.

3. Experimental

3.1. Synthesis of metal hexacyanocobaltates

The compounds are abbreviated as $[\text{M-Co}]$ throughout the manuscript. A similar synthetic approach to the reports previously was used for PBAs.²⁰

3.2. Preparation of catalyst modified electrodes

FTO electrodes (1×2 cm, 2 mm slides with $7 \Omega/\text{sq}^{-1}$ surface resistivity and $\sim 80\%$ transmittance) were washed by sonication for 10 min in basic soapy solution, deionized water and isopropanol, followed by annealing at 400°C for 30 min. Catalyst-modified electrodes were prepared by drop casting method. A mixture of 5 mg of PBA catalyst, 500 μL DMF, 500 μL water, and 100 μL Nafion solution were mixed and sonicated for 30

minutes. After making a stable suspension, 50 μL of it was taken and dropped onto the mixture by covering 1 cm^2 of the FTO electrode. Electrodes were then dried at room temperature for 10 min followed by 80 $^\circ\text{C}$ for 10 min in an oven. They were then left in desiccator until further use for electrochemical experiments and characterization.

3.3. Electrochemical section

A conventional three-electrode electrochemical cell was used with Ag/AgCl electrode (3.5 M KCl) as the reference electrode, Pt wire as counter electrode, and FTO spin coated with the PBA as working electrode. Neutral buffer solutions were prepared using K_2HPO_4 and KH_2PO_4 (KPi) and then adjusted by adding H_3PO_4 or KOH to desired pH. CVs were recorded with a scan rate of 100 mVs^{-1} in 50 mM KPi (pH 7) containing 1 M KNO_3 as electrolyte between 0 and 1.5 V (vs. Ag/AgCl). All experiments were carried out under nitrogen atmosphere. pH of the solution was measured by Mettler Toledo pH meter (S220).

3.4. Bulk water electrolysis and Tafel analysis

Bulk water electrolysis studies were performed with two-compartment cell with a glass frit separation. Pt wire counter electrode was placed in one compartment while FTO spin-coated with PBA working electrode and Ag/AgCl reference electrode were placed in the other compartment. The electrolysis experiments were carried out in KPi buffer (pH 7.0) solution containing 1 M KNO_3 as supporting electrolyte. Tafel data were collected in the same conditions at different applied potentials using steady current density of an equilibrium time of 600 s. Oxygen evolution was indirectly determined from pH changes of solution during bulk electrolysis in the absence of buffer solution (1 M KCl).

Acknowledgment

Funding from TÜBİTAK is gratefully acknowledged under the project 215Z249.

References

1. Ghobadi, T. G. U.; Ghobadi, A.; Ozbay, E.; Karadas, F. *ChemPhotoChem* **2018**, *2*, 161-182.
2. Wang, M.; Chen, L.; Sun, L. *Energy Environ. Sci.* **2012**, *5*, 6763-6778.
3. Concepcion, Javier J.; Houser, Ralph L.; Papanikolas, John M.; Meyer, T. J.; Concepcion, J. J.; House, R. L.; Papanikolas, J. M.; Meyer, T. J. *PNAS* **2012**, *109*, 15560-15564.
4. House, R. L.; Iha, N. Y. M.; Coppo, R. L.; Alibabaei, L.; Sherman, B. D.; Kang, P.; Brennaman, M. K.; Hoertz, P. G.; Meyer, T. J. *J. Photochem. Photobiol. C Photochem. Rev.* **2015**, *25*, 32-45.
5. Galán-Mascarós, J. R. *ChemElectroChem* **2015**, *2*, 37-50.
6. Roger, I.; Shipman, M. A.; Symes, M. D. *Nat. Rev. Chem.* **2017**, *1*, 3.
7. Kärkäs, M. D.; Åkermark, B. *Dalt. Trans.* **2016**, *45*, 14421-14461.
8. McCrory, C. C. L.; Jung, S.; Peters, J. C.; Jaramillo, T. F. *J. Am. Chem. Soc.* **2013**, *135*, 16977-16987.
9. Wasylenko, D. J.; Ganesamoorthy, C.; Borau-Garcia, J.; Berlinguette, C. P. *Chem. Commun. (Camb)*. **2011**, *47*, 4249-4251.
10. Dogutan, D. K.; Stoian, S. A.; McGuire, R.; Schwalbe, M.; Teets, T. S.; Nocera, D. G. *J. Am. Chem. Soc.* **2011**, *133*, 131-140.
11. Alsaç, E. P.; Ulker, E.; Nune, S. V. K.; Karadas, F. *Catal. Letters* **2018**, *148*, 531-538.

12. Nune, S. V. K.; Basaran, A. T.; Ülker, E.; Mishra, R.; Karadas, F. *ChemCatChem* **2017**, *9*, 300-307.
13. Ressnig, D.; Shalom, M.; Patscheider, J.; Moré, R.; Evangelisti, F.; Antonietti, M.; Patzke, G. R. *J. Mater. Chem. A* **2015**, *3*, 5072-5082.
14. Yamada, Y.; Oyama, K.; Gates, R.; Fukuzumi, S. *Angew. Chemie - Int. Ed.* **2015**, *54*, 5613-5617.
15. Goberna-Ferrón, S.; Hernández, W. Y.; Rodríguez-García, B.; Galán-Mascarós, J. R. *ACS Catal.* **2014**, *4*, 1637-1641.
16. Pintado, S.; Goberna-Ferrón, S.; Escudero-Adán, E. C.; Galán-Mascarós, J. R. *J. Am. Chem. Soc.* **2013**, *135*, 13270-13273.
17. Han, L.; Tang, P.; Reyes-Carmona, A.; Rodriguez-Garcia, B.; Torrens, M.; Morante, J. R.; Arbiol, J.; Galán-Mascarós, J. R. *J. Am. Chem. Soc.* **2016**, *138*, 16037-16045.
18. Yamada, Y.; Oyama, K.; Suenobu, T.; Fukuzumi, S. *Chem. Commun.* **2017**, *14*, 224-232.
19. Dunbar, K. R.; Heintz, R. A. *Prog. Inorg. Chem.* **1997**, *45*, 283-392.
20. Alsaç, E. P.; Ülker, E.; Nune, S. V. K.; Dede, Y.; Karadas, F. *Chem. Eur. J.* **2018**, *24*, 4856-4863.
21. Nakamoto, K. In *Handbook of Vibrational Spectroscopy*; John Wiley & Sons Ltd: Hoboken, NJ, USA, 2006.
22. Aksoy, M.; Nune, S. V. K.; Karadas, F. *Inorg. Chem.* **2016**, *55*, 4301-4307.
23. Ahn, H. S.; Tilley, T. D. *Adv. Funct. Mater.* **2013**, *23*, 227-233.
24. Sun, Y.; Liu, C.; Grauer, D. C.; Yano, J.; Long, J. R.; Yang, P.; Chang, C. J. *J. Am. Chem. Soc.* **2013**, *135*, 17699-17702.
25. Pintado, S.; Goberna-Ferrón, S.; Escudero-Adán, E. C.; Galán-Mascarós, J. R. *J. Am. Chem. Soc.* **2013**, *135*, 13270-13273.
26. Li, T.-T.; Cao, S.; Yang, C.; Chen, Y.; Lv, X.-J.; Fu, W.-F. *Inorg. Chem.* **2015**, *54*, 3061-3067.
27. Zaharieva, I.; Chernev, P.; Risch, M.; Klingan, K.; Kohlhoff, M.; Fischer, A.; Dau, H. *Energy Environ. Sci.* **2012**, *5*, 7081-7089.
28. Indra, A.; Menezes, P. W.; Zaharieva, I.; Baktash, E.; Pfrommer, J.; Schwarze, M.; Dau, H.; Driess, M. *Angew. Chemie Int. Ed.* **2013**, *52*, 13206-13210.